Lateral change of in-plate stress and seismicity along the southern Mariana trench

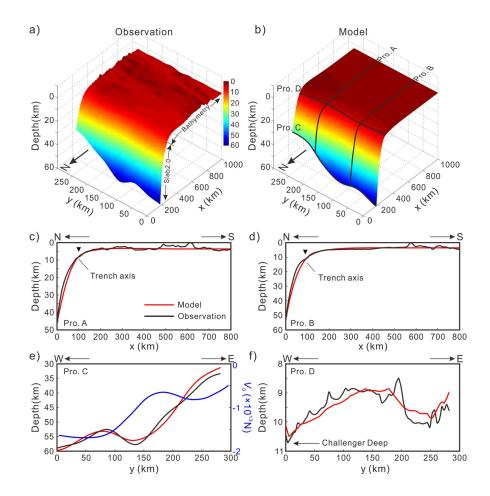
Jiangyang Zhang¹, Hongfeng Yang², Han Chen², Fan Zhang³, Gaohua Zhu², and Zhen Sun⁴

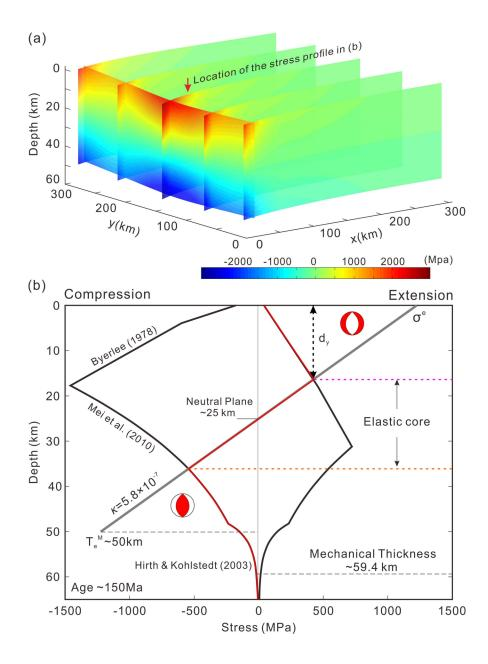
¹South China Sea Institute Of Oceanology
²The Chinese University of Hong Kong
³South China Sea Institute of Oceanology, Chinese Academy of Sciences
⁴CAS Key Laboratory of Ocean and Marginal Sea Geology, South China Sea Institute of Oceanology

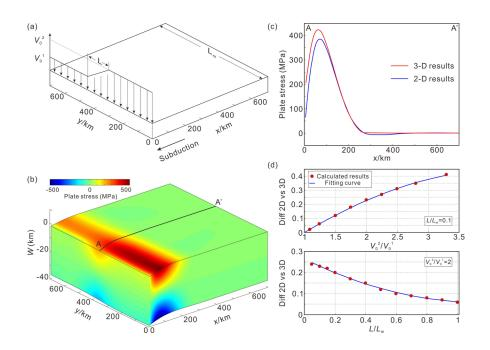
November 23, 2022

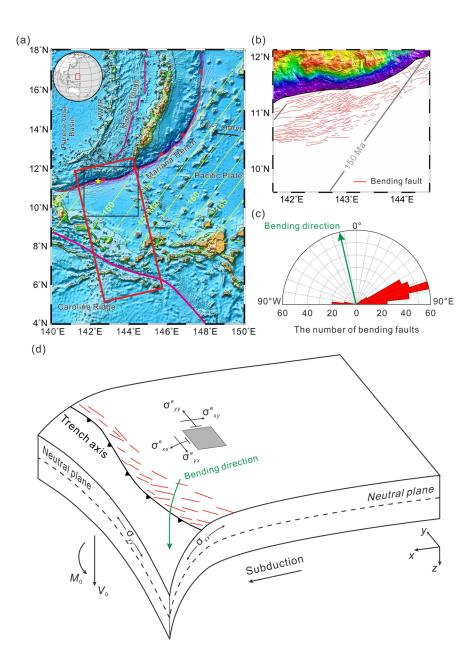
Abstract

Lithospheric flexure at subduction zones is a major contributor to induce outer rise earthquakes. Here, we modeled the bending deformation of the subducting plate at the southern Mariana using a 3-D plate flexural model. Intraplate stresses were investigated, with the along-strike variable boundary loadings. In order to match the observations of plate geometry, boundary vertical loading near the Challenger Deep has to be set twice of that in other areas. We also compared results between 2-D and 3-D models and found that the difference on estimating plate stress can exceed 20% when there is an along-strike variation in plate bending. Finally, we found that the sharp lateral variation in the σ and the σ corresponded to an outer rise earthquake cluster at the southern Mariana subduction zone, indicating that along-strike variation in σ and σ may be a significant mechanism to cause non-uniform distribution of outer rise earthquakes.









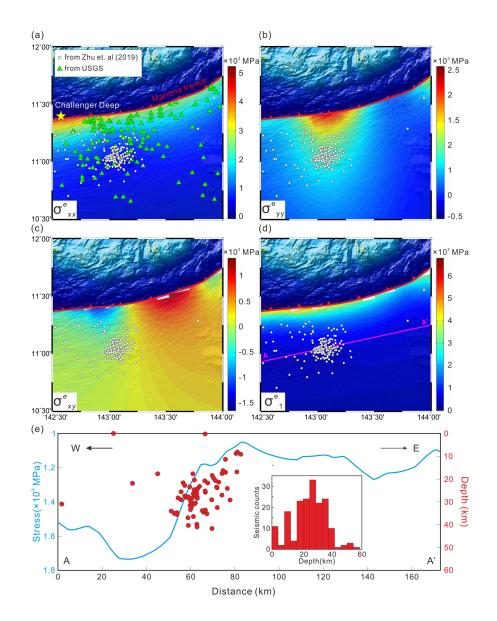


Figure01.

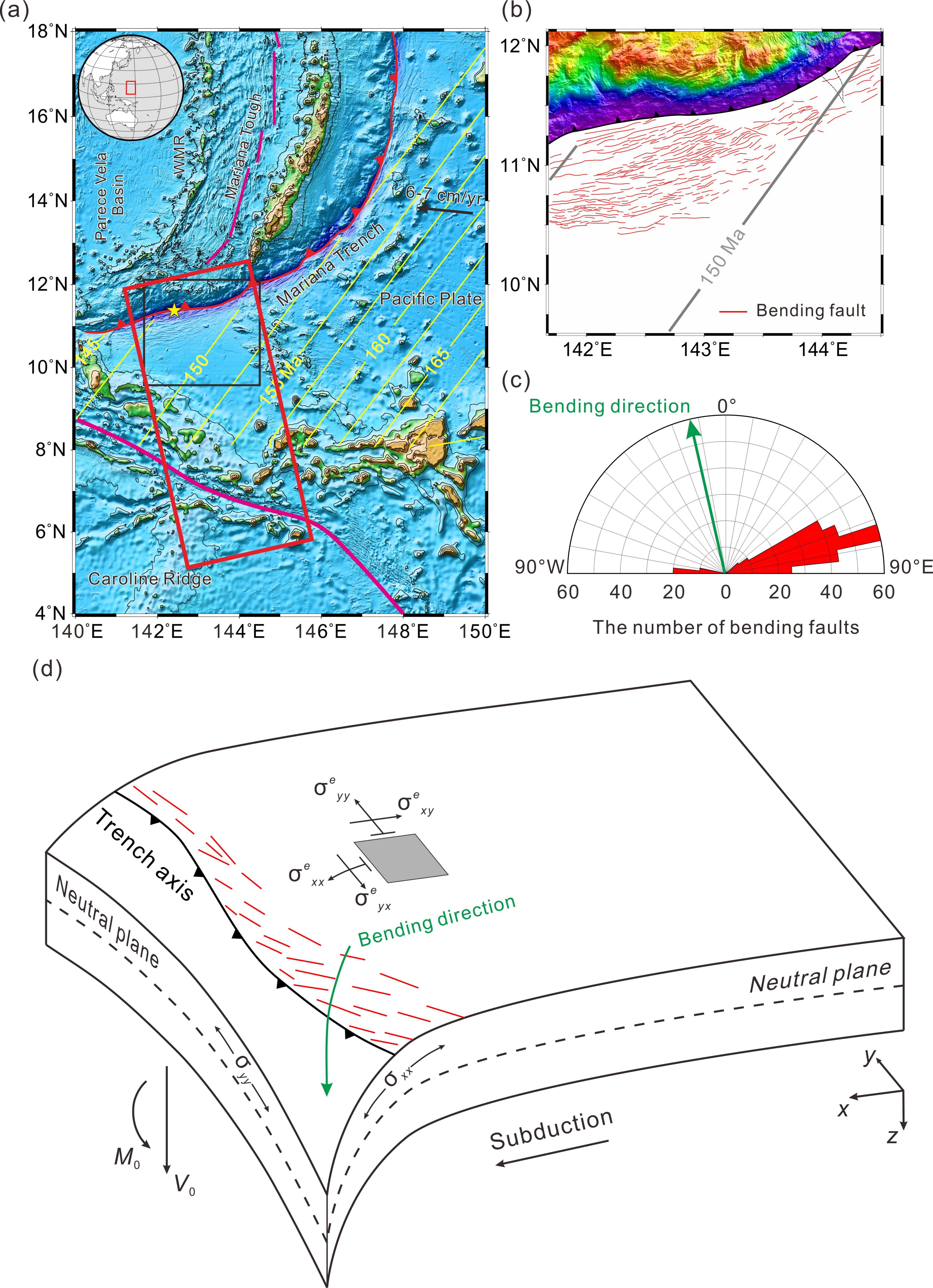


Figure02.

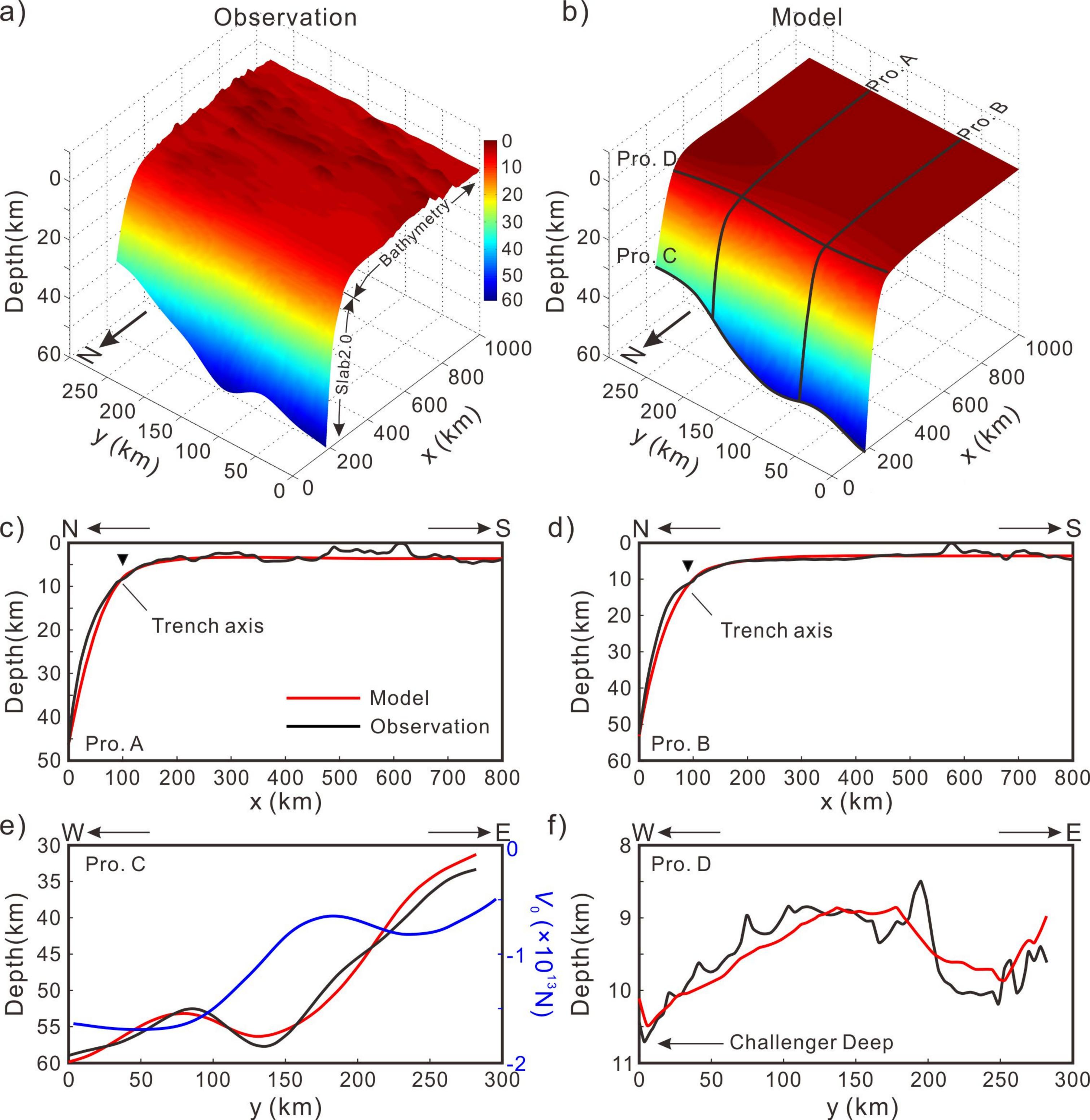
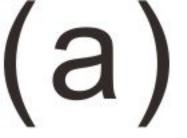


Figure03.



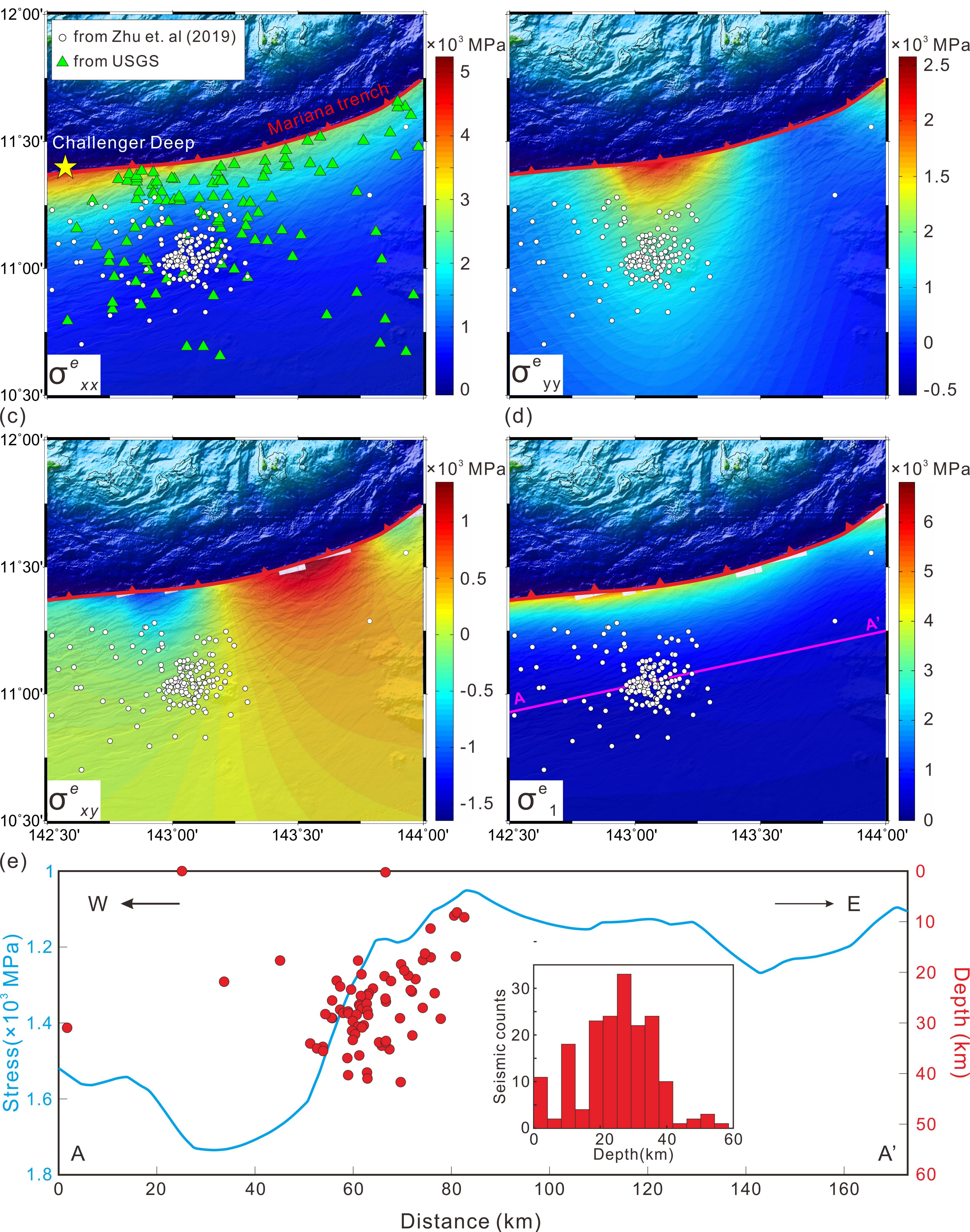
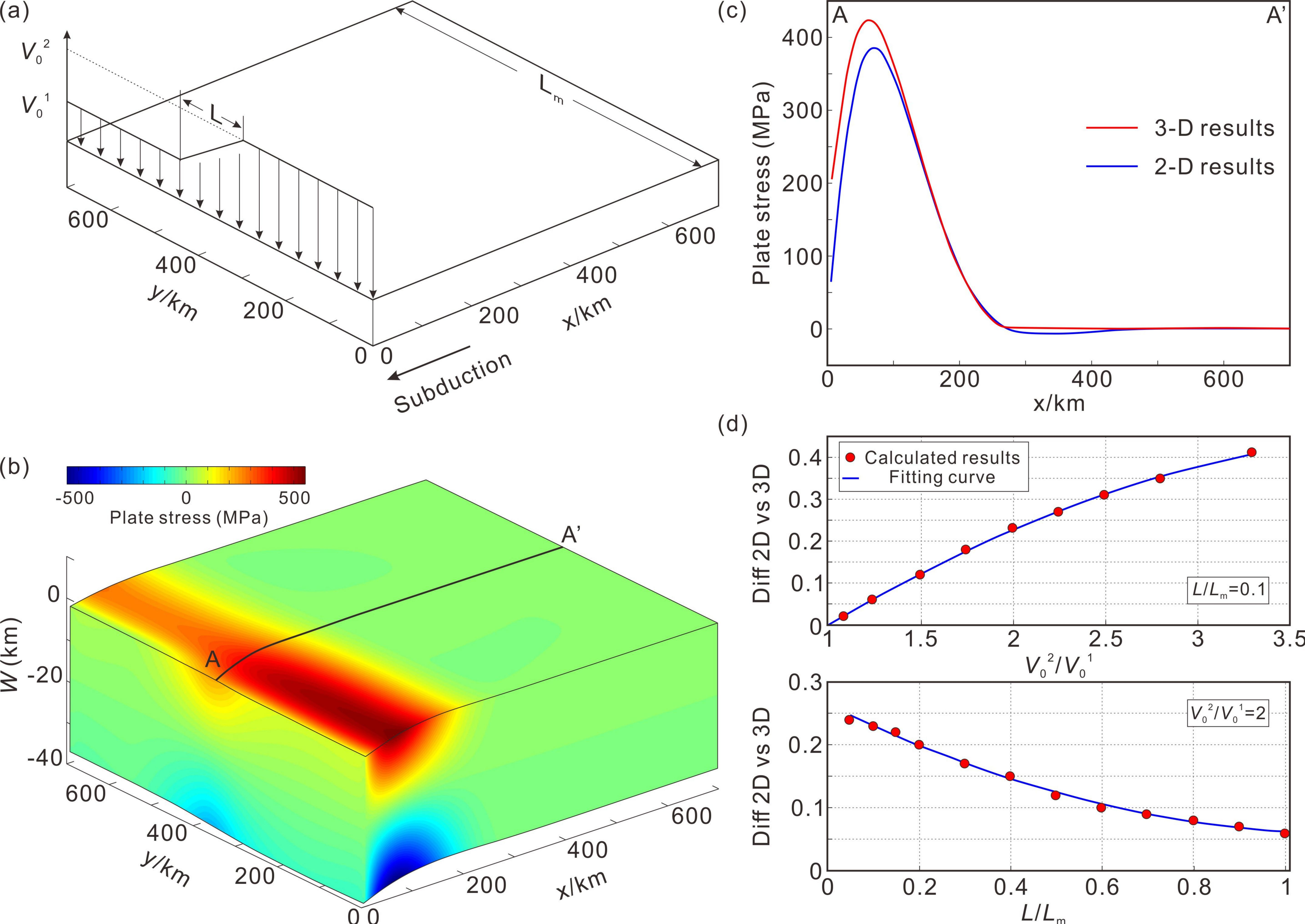


Figure04.



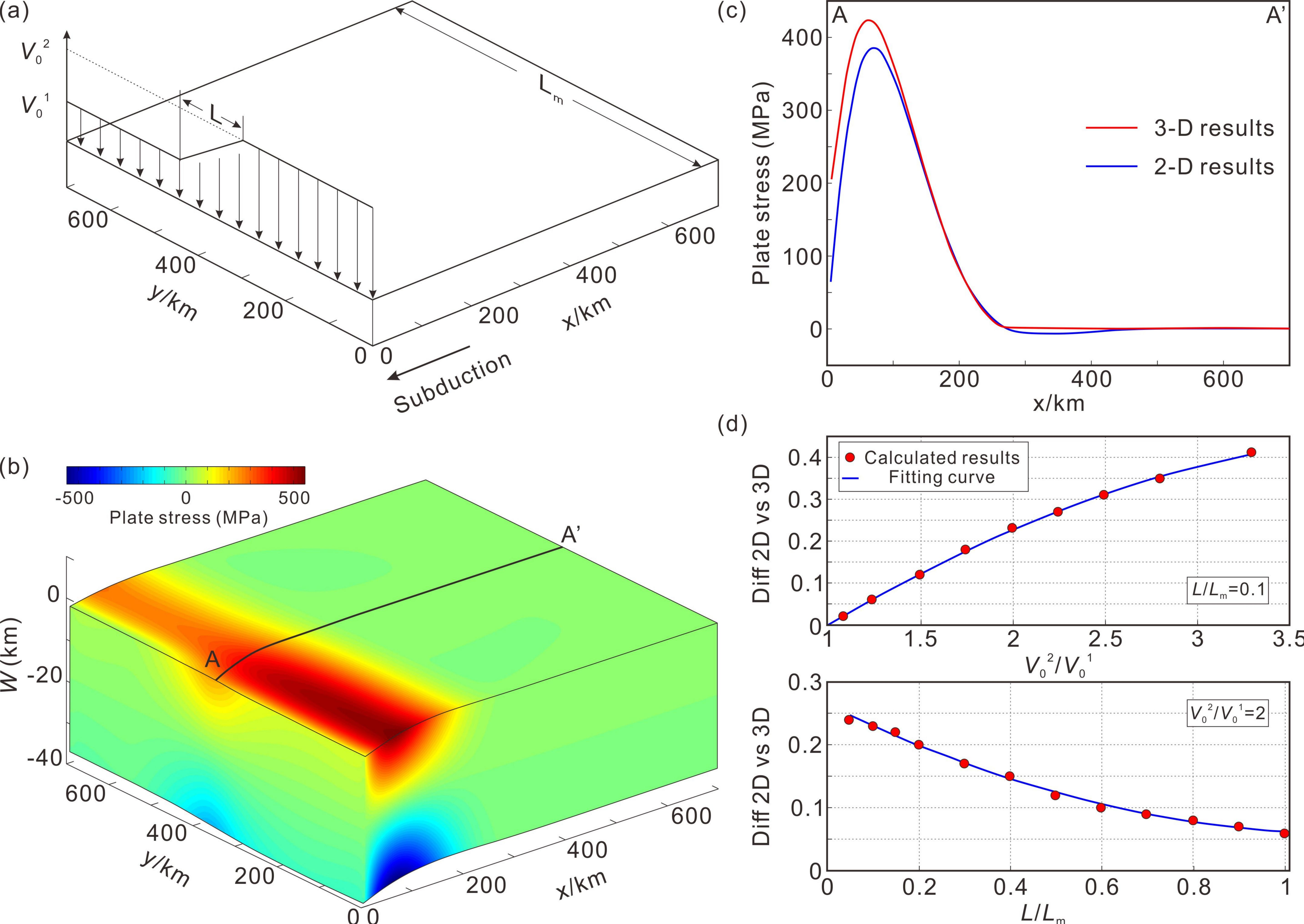
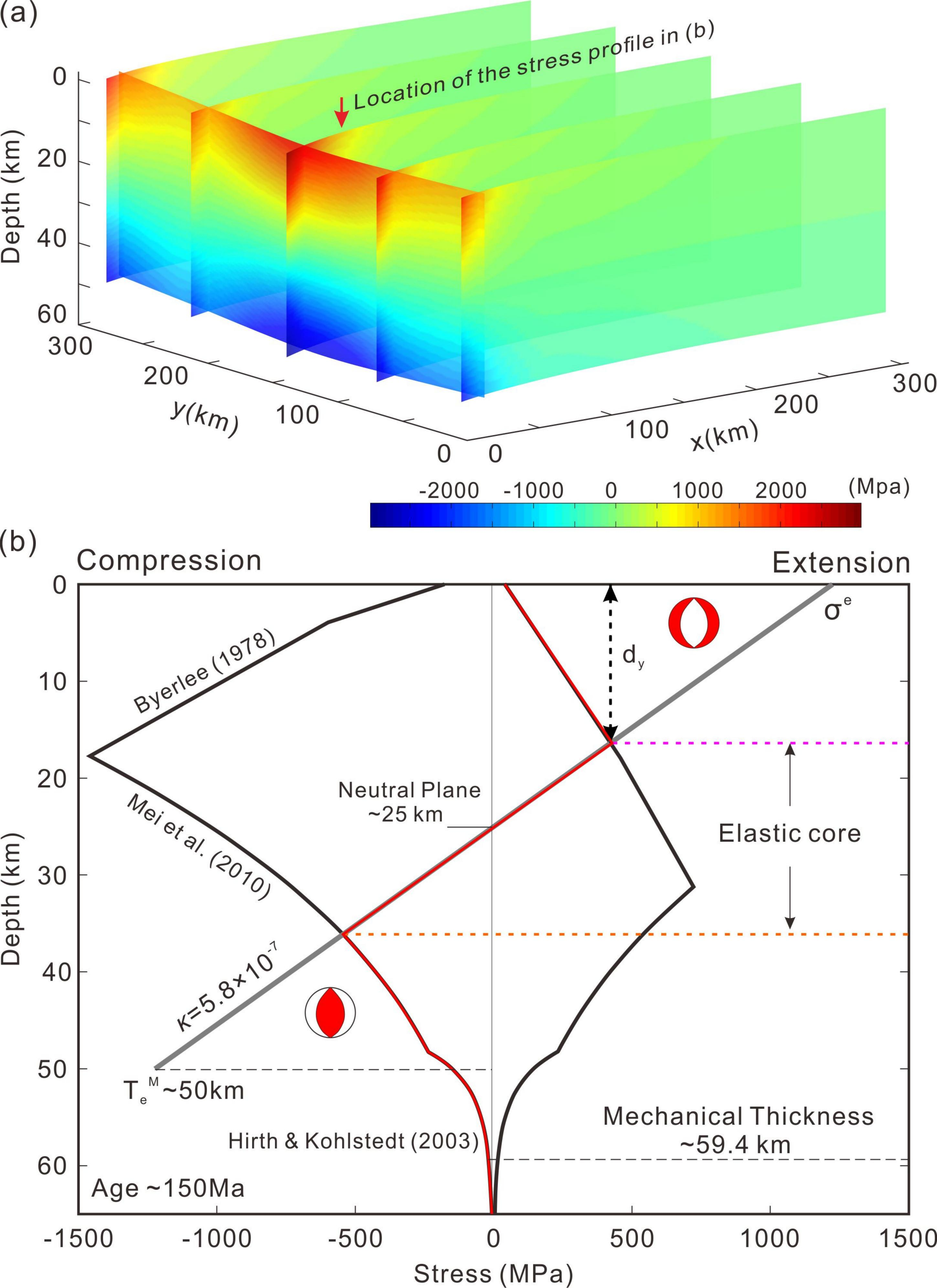


Figure05.



1	Lateral change of in-plate stress and seismicity along the				
2	southern Mariana trench				
3	Jiangyang Zhang ^{1, 2} , Hongfeng Yang ^{2, 1} *, Han Chen ² , Fan Zhang ³ ,				
4	Gaohua Zhu ² , and Zhen Sun ³				
5	¹ . Shenzhen Research Institute, The Chinese University of Hong Kong, Shenzhen,				
6	518057, China				
7	² . Earth System Science Programme, The Chinese University of Hong Kong, Shatin, NT,				
8	Hong Kong, China.				
9	³ . CAS Key Laboratory of Ocean and Marginal Sea Geology, Chinese Academy of				
10	Sciences, South China Sea Institute of Oceanology, Guangzhou 510301, China.				
11	* Corresponding author, Hongfeng Yang (hyang@cuhk.edu.hk)				
12	Abstract				
13	Lithospheric flexure at subduction zones is a major contributor to induce outer rise				
14	earthquakes. Here, we modeled the bending deformation of the subducting plate at the				
15	southern Mariana using a 3-D plate flexural model. Intraplate stresses were investigated,				
16	with the along-strike variable boundary loadings. In order to match the observations of				
17	plate geometry, boundary vertical loading near the Challenger Deep has to be set twice of				
18	that in other areas. We also compared results between 2-D and 3-D models and found				
19	that the difference on estimating plate stress can exceed 20% when there is an				
20	along-strike variation in plate bending. Finally, we found that the sharp lateral variation in				

the σ_{yy}^{e} and the σ_{xy}^{e} corresponded to an outer rise earthquake cluster at the southern Mariana subduction zone, indicating that along-strike variation in σ_{yy}^{e} and σ_{xy}^{e} may be a significant mechanism to cause non-uniform distribution of outer rise earthquakes.

24

Plain Language Summary

25 A subduction zone is a region where two tectonic plates converged. When a plate 26 is subducted beneath the other one and becomes bending, the accumulation of bending stress will occur. If the bending stress exceeds the yield strength of lithosphere, it will 27 28 induce the normal faults and earthquakes at outer rise. In our study, we simulated the 29 bending deformation of subducted plate at the southern Mariana subduction zone and 30 calculated corresponding stresses using the 3-D plate bending model. We found that 31 there is difference between the 2-D and 3-D model on estimating plate bending stress 32 when there is an along-strike variation of plate bending. We further found that the plate bending stress has very important relationship with the distribution of outer rise 33 34 earthquakes.

Key words: Mariana Subduction zone; Plate bending; Numerical simulation;
 Stress; Earthquakes

37 **1. Introduction**

Widely distributed subduction zone earthquakes may trigger large tsunami and cause significant loss of life and damage, as demonstrated by numerous examples (e.g. Gusman et al., 2009; Lay et al., 2010). In addition to interplate earthquakes, there are intra-plate earthquakes which could also be devastating, such as the 1977 Sumba

Indonesia (Sunda trench, M_w =8.3) (Lynnes and Lay, 1988), the 1990 Mariana Trench 42 43 $(M_w=7.3)$ (Yoshida et al., 1992), the 2007 Kuril Trench ($M_w=8.1$) (Ammon et al., 2008), and 44 the 2009 Somoa-Tonga (M_w=8.1, Beavan et al., 2010; Lay et al., 2010) earthquakes. All of these earthquakes occurred in the outer rise region seaward of trench in subduction 45 zones, where normal faults are generated or reactivated by plate bending 46 (Mortera-Gutiérrez et al., 2003; Ranero et al., 2003; 2005). An outer rise earthquake may 47 48 be triggered by a megathrust earthquake and sometimes may trigger a megathrust event 49 (Ammon et al., 2008; Beavan et al., 2010; Lay et al., 2010), enhancing the tsunami hazard 50 potential. Therefore, evaluating plate bending, stress distribution, and corresponding 51 earthquakes in the outer rise region are crucial to assess earthquake and tsunami hazard 52 in subduction zones.

53 Previous studies have recognized the important role of stress within the subducting plate in outer rise earthquakes (Chapple and Forsyth, 1979; Christensen and Ruff, 1983, 54 55 1988; Scholz and Small, 1995; Emry et al., 2014; Zhou et al., 2015, 2018). For instance, 56 Chapple and Forsyth (1979) explained the depths of tensional and compressional outer 57 rise earthquakes by using the idea that plate bending can produce tensional and 58 compressional stress regime, separated by a neutral plane. This model was supported by 59 focal mechanism solutions of outer rise earthquakes, e.g. along the Mariana subduction 60 zone where the focal depths of normal faulting events delineate the boundary between the extension and compression stress regimes (Emry et al., 2014). Zhang et al., (2014) 61 62 simulated the geometry of the subducted plate along the profile perpendicular to the 63 Mariana Trench using a two-segment effective elastic thickness (T_{e}) flexural model. They

suggested that the plate bending stresses could exceed the lithosphere yield strength envelope (YSE) resulting in faulting and tensional earthquakes in the upper plate, corresponding to the reduction in T_{e} . Their results showed a 21-61% reduction in T_{e} along the Mariana.

68 All of their work are based on 2-D flexural models, which only consider the bending or slab pull from the direction perpendicular to the trench and assume uniform stress 69 70 along the trench. However, recent works clearly show along-strike variation in distribution 71 of outer rise seismicity, e.g. the southern Mariana subduction zone (Zhu et al., 2019) 72 where pervasive normal faults are observed (Figure 1). Moreover, observations of 73 strike-slip earthquakes in outer rise further indicate complex stress fields and thus require 74 investigations considering laterally varying boundary conditions and loadings, rather than 75 2-D plate bending models.

76 Some 3-D plate bending models have been developed to investigate the subducted 77 plate geometry (Manríquez et al., 2014) and boundary loading variation (Zhang et al., 78 2018). However, no models have incorporated different aspects so as to provide 79 constraints on in-plate stress. Here we develop a 3D model by incorporating bathymetries of the incoming plate, geometries of the subducting slab, and varying loading conditions. 80 81 We then apply this model in the southern Mariana subduction zone and derive stress 82 distribution within the incoming plate, for the first time. The distribution of surface elastic stress is compared to the earthquake locations that were obtained from the recently 83 84 acquired seismic data (Zhu et al., 2019). In the end we discuss the possible relationship 85 between the plate bending, stress, and the distribution of outer rise normal fault 86 earthquakes.

87 2. Data and method

88 2.1. Data Preparation

Three kinds of data were used in our study, including 15 arc-second resolution 89 90 global bathymetry data (Olson et al., 2014) and local multibeam data with ~150m resolution (data from the NOAA website: https://www.ngdc.noaa.gov/maps/autogrid/), 91 92 global slabs geometry data (Slab 2.0 from Hayes et al., 2018), and newly acquired ocean 93 bottom seismic data (Zhu et al., 2019). Firstly, we identified the strike of the 94 bending-related normal faults from the multibeam data, as did in Ranero et al. (2005) for the Mid-America and the Chile Trench. Rose diagrams of the fault strike help us to 95 96 determine the bending direction of the plate (Figure1b and d). In order to make the plate 97 boundary parallel to the strike of normal fault, the model area was chosen following the bending direction (red rectangle in the Figure 1a). Then, the bathymetry data and Slab2.0 98 99 data are stitched together to provide well constraints on 3-D plate bending models.

100

2.2. Flexure model and inversion

101 It is widely accepted that the lithospheric plate is regarded as an elastic layer 102 floating on an inviscid layer and the flexure deformation can therefore be modeled by an 103 elastic thin plate under applied external forces (Watts, 2001; Turcotte and Schubert, 2014). 104 At subduction zones, if the strong plate bending exceeds the lithospheric yield strength, it 105 can result in bending-related normal faults, earthquakes and mantle serpentinization near the outer rise(Grevemeyeretal.2005; Ranero et al. 2005). This process may result in the
loss of strength and flexural rigidity of the lithosphere (Contreras-Reyes and Osses, 2010).
A plate bending model with variable flexural rigidity was therefore usually used to model
the deformation of the subducted plate (Zhang et al., 2014; Hunter and Watts, 2016;
Zhang et al., 2018).

The flexure model and inversion method used in this paper are similar to Zhang et 111 al., (2018). The plate deflection w was inverted by solving the 3-D plate flexure equation 112 113 with the finite difference method (FDM), as well as the Particle Swarm Optimization (PSO) 114 inversion method. The details of methodology have been described in Zhang et al., (2019). For simplicity, the T_e was divided into two parts (T_e^{M} and T_e^{m}) in our model similar to 115 previous studies (Contreras-Reyes and Osses, 2010; Zhang et al., 2014). The T_e^M 116 represents the seaward T_{e} where the curvature of plate is zero (Contreras-Reyes and 117 Osses, 2010) and the T_e^m stands for landward T_e deduced by normal faults and 118 serpentinization. Previous studies showed that the T_e of the oceanic plate at subduction 119 120 zone depends on plate age (Zhang et al., 2018). The age of subducting plate at southern Mariana subduction zone ranges from 145 to 150 MPa (Figure 1a and b), the T_e^M is 121 122 therefore set to a constant (50km) in our model.

The calculated area is set to a rectangle with *x* axis perpendicular to the trench and *y* axis along the trench (Figure 1d). The trench axis was set to be ~100km away from the boundary and the part landward of the trench was constrained by Slab2.0. Because the direction of trench strike is variable, if the curved trench was set to be the loading boundary, it may not be reflective of the bending direction of plate (Figure 1d). Choosing

the deep slab as the boundary has at least two advantages. One is that it keeps the outer 128 rise area away from the boundary, so the boundary effect can be avoided. The other one 129 130 is that it can help us handle the effect caused by the local topographic reliefs (such as seamounts) better, because our aim is to model the first-order deformation of the 131 132 subducting plate and the local topographic reliefs are noise that should be removed in our simulation. Both bending moment (M_0) and vertical shear force (V_0) vary along the 133 boundary. The squared RMS (root mean square) error W_{rms} between the observed data 134 135 and the modeled flexure is used to find the best-fit model.

136 2.3. In-plate stresses distribution

For the thin elastic plates, the components of the plane stress along the *x* and *y* axis
depending on the distance from the neutral plane (*z*) are given by:

139
$$\begin{bmatrix} \sigma_{xx} \\ \sigma_{yy} \\ \tau_{xy} \end{bmatrix} = -\frac{Ez}{1+\mu} \begin{bmatrix} \frac{1}{1-\mu} & \frac{\mu}{1-\mu} & 0 \\ \frac{\mu}{1-\mu} & \frac{1}{1-\mu} & 0 \\ 0 & 0 & 1 \end{bmatrix} \begin{bmatrix} \frac{\partial^2 w}{\partial x^2} \\ \frac{\partial^2 w}{\partial y^2} \\ \frac{\partial^2 w}{\partial x \partial y} \end{bmatrix}$$
(1)

where *E* and μ represent the Young's modulus and the Poisson's ratio which are set to 7 × 10¹⁰ Pa and 0.25 respectively. When we discuss the elastic core and the depth of plastic deformation constrained by the YSE, these stress components need to be projected onto the principal stress axes by:

144

$$\sigma_{1} = \frac{\sigma_{xx} + \sigma_{yy}}{2} + \sqrt{\left(\frac{\sigma_{xx} - \sigma_{yy}}{2}\right)^{2} + \tau_{xy}^{2}}$$

$$\sigma_{2} = \frac{\sigma_{xx} + \sigma_{yy}}{2} - \sqrt{\left(\frac{\sigma_{xx} - \sigma_{yy}}{2}\right)^{2} + \tau_{xy}^{2}}$$
(2)

145 **3. Results**

146 3.1. Statistics of fault strike at outer rise

In the southern Mariana, the magnetic lineation is obvious oblique to the trench and the bending normal faults. So it is suggested that the bending normal faults in the southern Mariana have no clear relationship with spreading. We identified ~260 bending faults from the multibeam bathymetry data using the method similar to Ranero et al., 2005 (Figure 1b and c). The rose diagram shows that the main direction of the fault strike is NEE (Figure 1c) and thus the green arrow shows that the bending direction is NNW. These two directions help us to determine the geographical range of our model (Figure 1).

154 3.2. Plate bending

155 A series of numerical model have been performed for a range of boundary loadings and plate effective thickness. Finally we choose the best-fitting model with the W_{rms} less 156 than 1.5 km. We obtained smooth model results, including the 3-D simulated plate 157 158 deformation (Figure 2b) and different profiles (Figure 2c-f). The red lines show the results of our model and the black lines are observed data. Profiles perpendicular to the trench 159 showed a ~1 km deviation between observations and our modeling results within 0 to 160 100km (Figure 2c and d). This may be caused by the discontinuity of the two datasets as 161 162 the precision of Slab2.0 is much lower than that of bathymetry. However, we believe that 163 this deviation would not affect the accuracy of our model, because the scale of our model is far greater than ~1km. 164

165

Along the strike of the trench, we found that the flexural depth of the subducted

plate becomes deeper from east to west, with a sharp variation of depth at the ~150km along the trench axis (Figure 2a, b and e). Such along-strike variation may be associated with the deepest spot, Challenger Deep (Figure 2f). To match the plate deformation, along-strike variable loadings were applied on the plate boundary. The bending moment applied on the western part (near the Challenger Deep) is nearly twice as much as that of the eastern part.

172

3.3. Stresses and earthquakes distribution

173 According to equations (1) and (2), the distribution of surface elastic stress components σ^{e}_{xx} , σ^{e}_{yy} , σ^{e}_{xy} and the maximum principal stress σ^{e}_{1} are calculated in the 174 best-fitting model (Figure 3). The σ_{xx}^{e} stands for the normal stress along the x axis (the 175 direction perpendicular to the trench) caused by plate bending perpendicular to the trench 176 and it reaches maximum close to the trench axis. The σ^{e}_{vv} represents the normal stress 177 along the strike of the trench mainly caused by lateral flexural deformation of the plate (the 178 179 direction along the trench). This means if the flexure morphology of the plate is invariant along the strike of the trench, the σ^{e}_{yy} will present the same tendency with σ^{e}_{xx} due to the 180 Poisson's ratio of materials. Conversely, if the flexure morphology of plate varies along the 181 strike of the trench, the σ_{vv}^{e} will change due to the lateral plate pull. The σ_{vv}^{e} represents 182 the shear force also caused by the lateral plate pull. If no lateral plate pulling exists, the 183 σ^{e}_{xy} will be zero. 184

185 We found that the stress distribution associated with the plate bending is 186 heterogeneous. In addition, the σ_{xx}^{e} increases gradually from the outer rise to the trench

187	and reaches the maximum at the Challenger Deep, consistent with previous studies
188	(Zhang et al., 2014, 2019). The $\sigma^{e}_{\ xy}$ variations from extension to compression (or the
189	opposite) and The σ^{e}_{yy} shows a high value at ~143 $^{\circ}$ E, 11-11.5 $^{\circ}N.$ Among the stress
190	components, the σ^{e}_{xx} is the largest, reaching the maximum of ~5GPa. The maximum of
191	$\sigma^{e}_{\ 1}$ exceeds 6GPa. Along the red line in Figure 3d, the depth of earthquakes and the
192	variation of σ^{e}_{1} were projected onto the profile in Figure 3e. It shows that from west to east,
193	there is a sudden drop of the $\sigma^e_{\ 1}$ at the distance ~40 - 60km (please note the stress axis is
194	reversed) and most of the earthquakes occur at this area. The depths of the earthquakes
195	vary from 0 to ~60km with the mode number of depth ~26km (the histogram in Figure 3e).

196 **4. Discussion**

197 4.1. Comparison between the 2-D and the 3-D model on estimating the plate stress

The stress distribution of the flexural lithosphere could be predicted by the curvature 198 of the 2-D profile perpendicular to the trench (Hunter et al., 2016; Zhang et al., 2019). The 199 200 plate stress distribution can further help us constrain the lithospheric yield zone, the depth of outer rise earthquakes and mantle serpentinization (Emry et al., 2014; Zhang et al., 201 2019). Garcia et al. (2019) suggested that the amount of strain ε (as well as the stress σ) 202 of a flexural plate can be described by: $\varepsilon = -Z \frac{\partial^2 W}{\partial x^2}$, where x is a horizontal coordinate 203 axis along the direction of maximum curvature. If the flexural parameters (such as M_0 and 204 V_0) are invariant along trench, the direction of maximum curvature is perpendicular to the 205 trench and the plate stress estimated by the 2-D model is nearly equal to that estimated 206

by the 3-D model. However, if the flexural parameters vary along trench, the direction of maximum curvature will change and point to the lowest place of the three-dimensional space. At this situation, the plate stress estimated by the 2-D profile curvature may be underestimated.

211 Figure 4 is an example that illustrates how along-strike variable V_0 generates the underestimated 2-D plate stress. Here, the V_0 is set to sectioned linear variation along the 212 strike, which means that the V_0 change from V_0^1 to V_0^2 linearly within a variation distance 213 L (Figure 4a). As we only consider the effects of the along-strike variable V_0 , the T_e was 214 215 set to a constant value (35km) here. Then we compared the difference between the 2-D and the 3-D model on estimating plate stress (Figure 4c). After employing dozens of 216 different calculation models, we found that both the change in V_0 and the variation 217 218 distance L (we used L/L_m in Figure 4d, where Lm is the width of our model) can affect the 219 difference between the 2-D and the 3-D model. It shows that the difference between the 2-D and 3-D the model on estimating plate stress increases with change of V_0 and 220 221 decrease with the variation distance L (Figure 4d). Considering the Mariana Trench, if the L/L_m equals to 0.1 and V_0^2/V_0^1 is set to 2, the difference between the 2-D and the 3-D 222 223 model can exceed 20% (Figure 4).

224

4.2. Surface elastic stress and the YSE

The in-plate stress of the elastic plate is linearly correlated with the distance from the neutral plane of the plate (z) (Equation 1). It means that the stress varies linearly from the maximum compressive stress to the Maximum tensile stress along the traversal section of a bending plate. However, the lithosphere is not perfect elastic. It will be yield
and generate plastic deformation (such as normal fault) when the stress exceeds the yield
strength of the lithosphere.

The stress distributions along different profiles at the South Mariana Trench in our 231 232 model are shown in Figure 5a. If the subducted plate is the ideal pure elastic material, the surface elastic stress can reach ~3GPa. While the actual plate bending stress is of limited 233 by the YSE. The YSE used in our study is combination of Beyerlee (1978), Mei et al. 234 235 (2010) and Hirth and Kohlstedt (2003) (Figure 5b). In Figure 5b, the grey line represents 236 the elastic stress profile at the location pointed by the red arrow in Figure 5a. σ^{e} is the surface elastic stress and d_v is the depth of the yield zone. Clearly, the d_v is linearly 237 positively correlated to the σ^{e} . It means that if the σ^{e} is given at anyplace, the d_v can be 238 239 estimated easily. Therefore, we can use the simulated surface elastic stress to constraint 240 the potential first fracture zone and the distribution of outer rise earthquakes.

4.3. Lateral variation of in-plate stress and outer rise earthquakes

Along the strike of the Mariana trench, the distribution of outer rise earthquakes is always non-uniform (Zhu et al., 2019). Christensen and Ruff (1988) proposed a model by considering the regional and plate bending stress to explain such phenomena. They indicated that although the lithospheric bending played a major role in inducing outer rise tensional earthquakes by placing the shallow region of outer rise in extension and causing brittle deformation, the regional compressional stress caused by the interaction between the upper and subducted plate can reduce the possibility of outer rise extensional events, such as the alternation of tensional and compressional outer rise earthquakes along the Kuril subduction zone (Ammon et al., 2008). However, previous studies have demonstrated a weak plate coupling at the southernmost Mariana Trench (Gvirtzman and Stern, 2004; Emry et al., 2014). It is unlikely that the uneven distribution of outer rise earthquakes located by Zhu et al., (2019) can be explained by the coupling between the upper and subducted plates.

Here, we proposed another possible mechanism which causes the variable 255 256 distribution of outer rise earthquakes - the lateral variation of in-plate stress. If there is a 257 variable boundary loading caused by deep slab pull, it will lead to the along-strike variable 258 bending depth as well as the variable plate bending stress at outer rise. We propose that 259 the bending stresses exceed the yield strength of the lithosphere due to the variable 260 loading, corresponding to the variable distribution of outer rise seismicity. Here the 261 bending stress includes not only the stress along the direction perpendicular to the trench but also the stress along the strike of the trench (σ^{e}_{yy} and σ^{e}_{xy}) caused by the laterally 262 263 plate pull. Actually, we found that the along-strike stress plays an unneglectable role in 264 deciding the distribution of outer rise earthquakes. For example at the southern Mariana Trench, it is hard to explain the concentrated outer rise seismicity only by the extensional 265 266 stress along the direction perpendicular to the trench. However, a sharp variation of the normal stress along the strike of the trench ($\sigma^{e}_{_{yy}}$) occurred just at the concentrated 267 seismic zone (Figure 3b). 268

269 **5. Conclusion**

270 By analyzing the results of plate bending simulation, in-plate stress, and the 271 distribution of outer rise earthquakes, we show that the variable boundary loadings along the strike of southern Mariana Trench caused by deep slab pull can cause not only 272 273 along-strike variation in degree of plate bending, but also the along-strike variant in-plate stresses. The boundary loading applied at the Challenger Deep area is nearly twice as 274 275 much as that of other areas, which can make the difference between the 2-D and the 3-D model on estimating the plate stress exceed 20%. An outer rise zone with concentrated 276 277 earthquakes in the southern Mariana subduction zone corresponds to the sharp variation 278 in the along-strike normal stress and the plane shear stress. It is therefore suggested that 279 the 3-D effect of plate bending can be a mechanism to cause non-uniform distribution of 280 outer rise earthquakes along trench.

281

6. Acknowledgements

282 We are grateful to Prof. Jian Lin, Dr. Xiaohuan Jiang, Xiang Chen, Suli Yao, 283 Pengcheng Zhou and Junhao Song for useful discussion. We thank Zhongxian Zhao and 284 Zhiyuan Zhou for offering technical assistance. GMT (Wessel and Smith 1995) was used 285 to draw the topographic map. The bathymetry data can be found at the website: https://catalog.data.gov/dataset/srtm15-plus-estimated-topography-15-seconds-global-v1. 286 The multibeam data with ~150m resolution can be found at the NOAA website: 287 288 https://www.ngdc.noaa.gov/maps/autogrid/ and the global slabs geometry data Slab 2.0 can be found at https://www.sciencebase.gov/catalog/item/5aa1b00ee4b0b1c392e86467 289

290 (Hayes et al., 2018).

This research is supported by National Key R&D Program of China (Grant Number 2018YFC1503400), Hong Kong Research Grant Council Grants (No. 14313816), Faculty of Science at CUHK, China Postdoctoral Science Foundation (No. 2019M663119), the Guangdong NSF research team project (2017A030312002), and the National Science Foundation of China (No. 41976064).

296

297 Reference

- Ammon, C.J., Kanamori, H., Lay, T., 2008. A great earthquake doublet and seismic stress
 transfer cycle in the central Kuril islands. Nature 451, 561-566.
- Beaven, J., Wang, X., Holden, C., Wilson, K., Power, W., Prasetya, G., Bevis, M., Kautoke,
- 301 R., 2010. Near-simultaneous great earthquakes at Tongan megathrust and outer rise
- in September 2009. Nature 466, 959-963
- 303 Byerlee, J., 1978. Friction of rocks. Pure appl. Geophys. 116 (4-5), 615-626.
- 304 Chapple, W.M., Forsyth, D.W., 1979. Earthquakes and bending of plates at trenches. J.
- 305 Geophys. Res. 84 (B12), 6729-6749.
- Christensen, D.H., Ruff, L.J., 1983. Outer-rise earthquakes and seismic coupling.
 Geophys. Res. Lett. 10, 697-700.
- 308 Christensen, D.H., Ruff, L.J., 1988. Seismic Coupling and Outer Rise Earthquakes. J.
- 309 Geophys. Res. 93 (B11), 13,421-13,444.
- 310 Contreras-Reyes, E., Osses, A., 2010. Lithospheric flexure modelling seaward of the

- 311 Chile trench: implications for oceanic plate weakening in the Trench Outer Rise 312 region. Geophys. J. Int. 182 (1), 97-112.
- 313 Emry, E.L., Wiens, D.A., Garcia-Castellanos., 2014. Faulting within the Pacific plate at the
- 314 Mariana Trench: Implications for plate interface coupling and subduction of hydrous
- minerals. J. Geophys. Res. Solid Earth 119, 2076-3095.
- 316 Garcia, E.S., Sandwell, D.T., Bassett, D., 2019. Outer Trench Slope Flexure and Faulting
- at Pacific Basin Subduction Zones. Geophys. J. Int. DOI: 10.31223/osf.io/dbn8j.
- Grevemeyer, I., Kaul, N., Diaz-Naveas, J.L., Villinger, H., Ranero, C.R., Reichert, C., 2005.
- 319 Heat flow and bending-related faulting at subduction trenches: Case studies offshore
- of Nicaragua and Central Chile. Earth planet. Sci. Lett. 236, 238-248.
- 321 Gusman, A.R., Tanioka, Y., Matsumoto, H., Iwasaki, S-I., 2009. Analysis of the Tsunami
- 322 Generated by the Great 1977 Sumba Earthquake that Occurred in Indonesia. Bull.
- 323 Seismol. Soc. Am. 99 (4), 2169-2179.
- 324 Gvirtzman, Z., Stern, R.J., 2004. Bathymetry of Mariana trench-arc system and formation
- of the Challenger Deep as a consequence of weak plate coupling. Tectonics 23,
 TC2011.
- Hayes, G., 2018, Slab2 A Comprehensive Subduction Zone Geometry Model: U.S.
- 328 Geological Survey data release, https://doi.org/10.5066/F7PV6JNV.
- Hirth, G., Kohlstedt, D., 2003. Rheology of the Upper Mantle and the Mantle Wedge: A
- 330 View from the Experimentalists. in *Inside the Subduction Factory*, pp. 83-105, ed.
- 331 Eiler, J., American Geophysical Union.
- Hunter, J., Watts, A.B., 2016. Gravity anomalies, flexure and mantle rheology seaward of

333	circum-Pacific trenches.	Geophys. J.	Int. 207 ((1), 288-316.
-----	--------------------------	-------------	------------	---------------

- Lay, T., Ammon, C. J., Kanamori, H., Rivera, L., Koper, K. D., Hutko, A. R., 2010. The 2009 Samoa-Tonga great earthquake triggered doublet. Nature 466, 964–967.
- 336 Lay, T., Ye, L., Bai, Y., Cheung, K.F., Kanamori, H., 2018. The 2018 *M*_W 7.9 Gulf of Alaska
- Earthquake: Multiple Fault Rupture in the Pacific Plate. Geophys. Res. Lett. 45,
 9542–9551.
- Lynnes, C., Lay, T., 1988. Source process of the great Sumba earthquake. J. Geophys.
 Res. 93, 13,407-14,320.
- Manríquez, P., Contreras-Reyes, E., Osses, A., 2014. Lithospheric 3-D flexure modelling
- of the oceanic plate seaward of the trench using variable elastic thickness. Geophys.J. Int. 196, 681–693.
- Mei, S., Suzuki, A.M., Kohlstedt, D.L., Dixon, N.A., Durham, W.B., 2010. Experimental
- constraints on the strength of the lithospheric mantle. J. Geophys. Res. 115 (B8).
- 346 Mortera-Gutiérrez, C.A., Scholl, D.W., Carlson, R.L., 2003. Fault trends on the seaward
- 347 slope of the Aleutian Trench: Implications for a laterally changing stress field tied to a
- 348 westward increase in oblique convergence. J. Geophys. Res. 108, 2477.
- 349 Ranero, C.R., Morgan, J.P., McIntosh, K., Reichert, C., 2003. Bending-related faulting and
- mantle serpentinization at the Middle America trench. Nature 425(6956), 367–373.
- 351 Ranero, C.R., Villaseñor, A., Morgan, J.P., Weinrebe, W., 2005. Relationship between
- bending-faulting at trenches and intermediate-depth seismicity. Geochem. Geophys.
- 353 Geosyst. 6 (12).
- 354 Scholz, C. H., Campos, J., 1995. On the mechanism of seismic decoupling and back arc

- spreading at subduction zones, J. Geophys. Res., 100 (B11), 22,103–22,115.
- Turcotte, D., Schubert, G., 2014. *Geodynamics*, 3nd edn. Cambridge University Press, pp.
 626.
- 358 Watts, A.B., 2001. *Isostasy and Flexure of the Lithosphere*, 1st edn, Cambridge University
- 359 Press, New York, pp. 478.
- 360 Yoshida, Y., Satake, K., Abe, K., 1992. The large normal-faulting Mariana Earthquake of
- April 5, 1990 in uncoupled subduction zone. Geophys. Res. Lett. 19 (3), 297-300.
- 362 Zhang, F., Lin, J., Zhan, W., 2014. Variations in oceanic plate bending along the Mariana
- trench. Earth planet. Sci. Lett. 401, 206-214.
- Zhang, F., Lin, J., Zhou, Z., Yang, H., Zhan W., 2018a. Intra- and intertrench variations in
- flexural bending of the Manila, Mariana and global trenches: implications on plate
 weakening in controlling trench dynamics. Geophys. J. Int. 212, 1429-1449.
- Zhang, J., Sun, Z., Qiu, N., Zhang, Y., Li, F., 2019. 3-D effective elastic thickness inversion
- of subduction zone based on particle swarm optimization algorithm. Chinese J.
 Geophys. (in Chinese) 62 (12), 4738-4749.
- Zhang, J., Sun, Z., Xu, M., Yang, H., Zhang, Y., Li, F., 2018. Lithospheric 3-D flexural
- 371 modelling of subducted oceanic plate with variable effective elastic thickness along
- the Manila Trench. Geophys. J. Int. 215, 2071-2092.
- Zhou, Z., Lin, J., Behn, M.D., Olive, J.A., 2015. Mechanism for normal faulting in the
 subducting plate at the Mariana Trench. Geophys. Res. Lett. 42, 4309-4317.
- Zhou, Z., Lin, J., Elasto-plastic deformation and plate weakening due to normal faulting in
- the subducting plate along the Mariana Trench. Tectonophysics 734, 59-68.

Zhu, G., Yang, H., Lin, J., Zhou, Z., Xu, M., Sun, J., Wan, K., 2019. Along-strike variation
in slab geometry at the southern Mariana subduction zone revealed by seismicity
through ocean bottom seismic experiments. Geophys. J. Int. 218 (3), 2122-2135.

381 Figures

382 Figure 1. (a) Seafloor bathymetry of the southern Mariana Trench. The red rectangle is the domain of our 3-D flexural model; the black square box is the area where the normal faults 383 384 are identified with the multi-beam data (please see Figure 1b) and the yellow star 385 represents the location of the Challenger Deep. Yellow lines are the magnetic lineation 386 based on Zhou et al., (2015). (b) Tectonic structure of the oceanic plate. Red lines are normal faults identified from the multibeam. (c) The rose diagram (red part) shows that the 387 388 direction of strike of the bending-normal faults is NEE at the southern Marina Trench and the green arrow perpendicular to the fault strike shows that the bending direction is NNW. 389 390 (d) Schematic 3-D model to illustrate the bending stresses of subducted plate under 391 along-strike variable loadings (bending moment (M_0) and vertical shear force (V_0) caused by deep slab pull). σ_{xx} and σ_{yy} represent the stresses on vertical profiles. σ^{e}_{xx} , σ^{e}_{yy} , and 392 σ^{e}_{xy} are surface elastic stresses (The meaning of surface elastic stress is shown in Figure 393 6). 394

395

Figure 2. Result of our model. (a) Observed plate bending of the study area. (b) 3-D plate bending model results. Pro. A, B, C, and D represent the profiles shown in Fig 2c-f. The

Pro. D is along the trench axis. (c)-(f) Comparisons between our model and observed data
along different profiles in Figure 2(b).

400

Figure 3. The components of the surface elastic stress (the meaning of the surface elastic 401 402 stress is shown in Figure 5). The white circles represent the location of outer rise earthquakes proposed by Zhu et al., (2019) and the grey crossing in Figure (a) are historic 403 outer rise earthquakes in this area (from USGS). (a) The distribution of σ^{e}_{xx} , the normal 404 405 stress along the direction perpendicular to the trench. The yellow star stands for the 406 location of the Challenger Deep. (b) The distribution of σ^{e}_{yy} , the normal stress along the strike of the trench, and (c) The distribution of the plane shear stress σ^{e}_{vv} . (d) The 407 distribution of the maximum principal stress σ_1^e (Please see the equation (2)). (e) The σ_1^e 408 409 and depth of outer rise earthquakes along the profile A-A' in Figure (d). It shows that the sharp variation of the σ^{e_1} along the strike of trench corresponds well to the concentrated 410 411 seismic zone. The histogram represents the variation of seismic depths.

412

Figure 4. The difference between the 2-D and the 3-D model on estimating the plate stress. (a) Schematic 3-D model to illustrate the along-strike variable V_0 . *L* is the variation distance of V_0 and L_m is the width of our model. (b) The 3-D plate stress distribution under the loading shown in Figure a. The difference of the surface elastic stress between the 2-D and the 3-D model along the profile A-A' in Figure b. (d) Plotting difference between the 2-D and the 3-D model on estimating plate stress versus the change of $V_0 (V_0^2/V_0^1)$ and the L/L_m

420

Figure 5. The relationship between the surface elastic stress and outer rise earthquakes. 421 422 (a) Profiles with different direction along the southern Mariana and their bending stress distributions. The red arrow is the location of the profile shown in Figure (b). (b) The YSE 423 424 used by Hunter and Watts (2016) which is a combination of the rheology laws of Byerlee 425 (1978), Mei et al. (2010), and Hirth and Kohlstedt (2003). The plate age at the southern 426 Mariana Trench is nearly 160 Ma with a mechanical thickness of ~59km. The grey line 427 represents the plate elastic stress profile and the red line represents the real stress profile due to plastic deformation. The σ^{e} is the surface elastic stress (a theoretical value in the 428 model) and the d_v is the yield depth. It is suggested that bending-related normal fault 429 (earthquake) occurred shallower than this depth. It shows that the σ^e is positively 430 correlated with the d_v and therefore the σ^e can be used to constrain the potential first 431 432 fracture zone.